

Optic Nerve Tortuosity, Globe Proptosis and Size Impact Retinal Ganglion Cell Thickness in General, Glaucoma and Myopic Populations

Charis Y.N. Chiang^{1,2,3}, Xiaofei Wang⁴, Stuart K. Gardiner⁵, Martin Buist², Michaël J.A. Girard^{1,3,6,7,8}

¹Department of Ophthalmology, Emory University School of Medicine, Atlanta, Georgia USA

²Department of Biomedical Engineering, National University of Singapore, Singapore

³Singapore Eye Research Institute, Singapore National Eye Centre, Singapore

⁴Key Laboratory for Biomechanics and Mechanobiology of Ministry of Education, Beijing Advanced Innovation Center for Biomedical Engineering, School of Biological Science and Medical Engineering, Beihang University, Beijing, China

⁵Devers Eye Institute, Legacy Health, Portland, Oregon, United States

⁶Department of Biomedical Engineering, Georgia Institute of Technology/Emory University, Atlanta, GA, USA

⁷Emory Empathetic AI for Health Institute, Emory University, Atlanta, GA, USA

⁸Duke-NUS Graduate Medical School, Singapore

Meeting Presentation: Presented in part at the Association for Research in Vision and Ophthalmology annual meeting, Seattle, USA, May 2024

Financial Support: Girard acknowledges support from Emory Eye Center (Start-up funds, MJAG), BrightFocus Foundation (G2021010S), TARGET (MOH-OFLCG21jun-0003) and Challenge Grant from Research to Prevent Blindness, Inc.

Financial Disclosure: No financial disclosure.

Conflict of Interest: MJAG is the co-founder of the start-up company Abyss Processing Pte Ltd.

Running Head: Impact of Orbit Structures on RNFL thickness

Keywords optic nerve tortuosity; globe proptosis; retinal nerve fiber layer thinning; glaucoma; myopia

List of Abbreviations: **AI** – Artificial Intelligence
GEE – Generalized Estimating Equations
ILPP – Interzygomatic Line-to- Posterior Pole
MRI – Magnetic Resonance Imaging
OCT – Optical Coherence Tomography
ONT – Optic Nerve Tortuosity
RGC – Retinal Ganglion Cell
RNFL – Retinal Nerve Fiber Layer

Word count: 3960 (manuscript text)

Tables: 4

Figures: 6

Supplemental Figure: 3

Corresponding Author: Dr Michaël J.A. Girard
Ophthalmic Engineering & Innovation Laboratory (OEIL), Emory Eye Center, Emory School of Medicine, Emory Clinic Building B, 1365B Clifton Road, NE, Atlanta GA 303
mgirard@ophthalmic.engineering
<https://www.ophthalmic.engineering>

Submission Date: 17/01/2025

ABSTRACT

Purpose: To investigate the impact of optic nerve tortuosity (ONT), and the interaction of globe proptosis and globe size on retinal ganglion cell (RGC) thickness, using Retinal Nerve Fiber Layer (RNFL) thickness, across general, glaucoma, and myopic populations.

Design: Cross-Sectional Study

Participants. This study analyzed 17970 eyes from the UKBiobank cohort (ID 76442), including 371 and 2481 eyes from glaucoma and myopia patients respectively.

Methods: Artificial intelligence models were trained to segment relevant structures from 3D optical coherence tomography (OCT) scans and 3D T1 magnetic resonance images (MRI). RNFL thickness, with and without correction for ocular magnification, was derived from OCT scans. MRI parameters included ONT, globe proptosis, axial length, and a novel feature: the interzygomatic line-to-posterior pole (ILPP) distance – a composite marker of globe proptosis and size. Generalized estimating equation (GEE) models evaluated associations between orbital and retinal features in all populations.

Main Outcome Measure: Associations between RNFL thickness and features of the orbit, primarily ONT and ILPP distance.

Results: Segmentation models achieved Dice coefficients over 0.94 for both MRI and OCT. RNFL thickness was positively correlated with ONT and ILPP distance ($r = 0.065$, $p < 0.001$, and $r = 0.206$, $p < 0.001$ respectively). The same was true for glaucoma ($r = 0.140$, $p < 0.01$, and $r = 0.256$, $p < 0.01$, for ONT and ILPP respectively), and for myopia ($r = 0.071$, $p < 0.001$, and $r = 0.100$, $p < 0.0001$, for ONT and ILPP respectively). GEE models revealed that straighter optic nerves and shorter ILPP distance were predictive of thinner RNFL in the general population, and in both disease subpopulations.

Conclusions: This study highlights the influence of ONT, as well as globe size and proptosis on retinal health. RNFL thinning may result from biomechanical stress due to straighter optic nerves or decreased ILPP distance, particularly in glaucoma and myopia. The novel ILPP metric integrates globe size and position, emerging as a potential biomarker of axonal health. These findings underscore the importance of orbit structures in RGC axonal health and warrant further research into the biomechanical interplay between the orbit and optic nerve.

INTRODUCTION

The optic nerve is essential for transmitting visual information from retinal ganglion cells (RGC) to the brain, and multiple studies suggest that mechanical forces acting on it may significantly impact RGC axonal health ¹. These studies, using techniques such as Optical Coherence Tomography (OCT), Finite Element modelling, and Magnetic Resonance Imaging (MRI), have identified the optic nerve head as particularly susceptible to deformation caused by optic nerve traction – a pulling force on the optic nerve induced by eye movements ^{2–10}. This traction is likely influenced by the structural characteristics of the orbit, which may, in turn, potentially compromise RGC axonal integrity, affecting both the nerve and the retinal nerve fibre layer (RNFL) ⁷. However, despite growing interest in this area, the interplay between the orbital structures and RGC axonal health remains poorly understood.

Understanding the factors influencing traction forces is particularly relevant to glaucoma, a leading cause of irreversible blindness, characterized by progressive loss of RGC axons and visual field loss ^{11,12}. Previous studies have highlighted two key orbital features associated with glaucoma: optic nerve geometry and globe size and/or position. First, Wang et al. found that glaucoma patients had less tortuous optic nerves across primary, abduction and adduction gazes compared to controls ⁸. Straighter nerves could increase RGC axonal stress during eye movements. The same study noted increased globe proptosis at primary gaze, which may elevate tension at the optic nerve head and exacerbate glaucomatous damage ⁸. Demer et al. reported abnormal globe retraction due to optic nerve tethering during adduction in glaucoma subjects, particularly in Asian eyes ^{7,10}. This may induce stress at the globe-optic nerve junction, aligning with Wang et al.'s findings of increased proptosis in Chinese glaucoma subjects ^{7,10}. Similarly, thyroid eye disease, a risk factor of glaucoma, has been associated with altered orbital mechanics and increased optic nerve strain in eyes with proptosed globes, reinforcing the potential impact of orbital influences on RGC axonal health ^{6,13}.

Additionally, optic nerve traction may partially contribute to myopia development. Wang et al. found that estimated optic nerve tortuosity (ONT) before myopic onset, was significantly lower in highly myopic eyes than measured ONT in controls suggesting that higher traction forces occur in eyes predisposed to myopia⁹. Chuangsuwanich et al. reported exaggerated intraocular pressure-induced strain in myopic eyes and positive correlation between adduction-induced strain at the and intraocular pressure-induced strain¹⁴. Given this and that optic nerve head connective tissues are weakened in myopic eyes^{15,16}, it is plausible that adduction-induced strain at the optic nerve head is elevated in myopia. These increased forces at the optic nerve head could contribute to RGC axonal loss in myopic, providing a potential explanation for myopia being a risk factor for glaucoma¹⁶.

Despite these findings, the full extent of how orbital structures influence axonal health remains underexplored, particularly in glaucoma and myopic. Notably, no studies to date have systematically examined the correlation between orbital structures and RGC axonal health. The UK Biobank initiative offers a unique opportunity to investigate these associations on a large scale with extensive population-wide imaging data, including brain MRIs (capturing the globe and orbit) and macular OCTs. Additionally, advances in artificial intelligence (AI) allow for the large-scale analysis of these complex relationships, Together, these facilitate the study of previously underexplored biomechanical factors through a population-wide study.

In this study, we aimed to elucidate the relationship between axonal health, surrogated by macular RNFL thickness, and specific orbital features. RNFL thickness is a non-invasive marker for axonal health, as thinner RNFLs indicate greater axonal degeneration^{17,18}. Additionally, we aimed to investigate the complex interactions among orbital parameters, and introduced a novel orbital feature that may provide a stronger correlation with RNFL thickness and offer potential for predicting its changes.

METHODS

Dataset Curation

This population study used demographic, diagnostic and imaging data from the UKBiobank cohort (ID 76442). The UK Biobank study is a large-scale, ongoing population study following 500,000 adult UK residents from 2010 onward. Disease information for subjects was encoded using the International Classification of Diseases (ICD-9 and ICD-10) codes. A subset of participants underwent macular OCT scans and structural brain MRIs.

The 3D spectral domain OCT scans were centered on the fovea, covering a 6mm x 6mm area using a raster scan protocol (3D OCT-1000 Mark II, Topcon, Japan). Each OCT volume was stored in FDS format and consisted of 128 B-scans at 47.2 μ m resolution, 512 A-scans per B-scan at 11.7 μ m resolution and 650 pixels per A-scan at an axial resolution of 3.5 μ m.

The T1-weighted structural brain MRI scans were acquired using a Siemens Skyra 3T system running VD13A SP4 (as of October 2015) with a 32-channel RF head coil. Scans covered the full head in 208 sagittal slices, each 256 x 256 pixels at a 1mm isotropic voxel resolution, over a 5-minute duration.

OCT and MRI scans from the UK Biobank were curated to include subjects with both an OCT scan (in at least one eye) and an MRI scan. Sex, disease diagnoses, and age at the time of scanning were recorded. The glaucoma subpopulation was identified based on ICD-9 and ICD-10 codes (Supplementary Note 1). We defined eyes with axial myopia, where axial length was greater than or equal to 25 mm, as belonging to the myopic subpopulation.

Measurement of Retinal Nerve Fibre Layer Thickness

To assess RNFL thickness, we developed a robust AI algorithm for segmenting retinal tissue structures from OCT scans before measuring RNFL thickness around the fovea. To this end, a total of 120 OCT B-scan images were randomly selected from 41 scan volumes across 27 subjects. Scans were image-compensated to improve contrast and tissue visibility using the methods described in our previous study ¹⁹. The compensated OCT images were then

manually segmented (Figure 1a) to identify the following tissue groups: (1) RNFL, (2) ganglion cell layer, (3) inner plexiform layer, (4) inner nuclear layer, (5) outer plexiform layer, (6) outer nuclear layer, (7) external limiting membrane, (8-11) four photoreceptor layers, (12) retinal pigment epithelium, and (13) choroid, with the background assigned a value of zero. In most images, the posterior choroid boundary was indistinct, and the sclera was not visible due to limited depth penetration; only visible tissues were segmented.

The manually segmented dataset was split into 85% for training and validation and 15% for testing. A cross-entropy loss function was used. As per the methods of our previous study ¹⁹, extensive data augmentation was applied to the training set, including horizontal flipping, random rotation and translation, additive Gaussian noise, and random saturations. A UNET++ model was then trained to automatically segment the tissue layers in the OCT images. Five-fold cross validation was performed, and the mean Dice coefficient metric was used to evaluate model performance.

RNFL thickness was measured as the minimum distance between the anterior and posterior boundaries (Figure 1b), with true values calculated by multiplying pixel counts by pixel resolution. The foveal center was identified using a modified gradient descent algorithm applied to a thickness map of the summed four inner layers. Average global RNFL thickness was calculated within a 1.5 mm radius of the fovea, excluding the central 0.5 mm, as well as for the superior, nasal, inferior, and temporal quadrants (Figure 1c).

Extraction of Orbit Features

To analyze the features in the orbit, we developed custom AI algorithms for automatic segmentation of key orbit structures from MRI scans and the subsequent extraction of relevant features from the segmented scans.

Segmentation of MRI Scans. MRI scans were cropped around each globe center to capture the entire globe, zygomatic bone, and visible optic nerve. The images were then resampled to 0.2 mm isotropic resolution using a Lanczos3 filter for precise segmentation, and left-eye volumes were horizontally flipped to match the orientation of right-eye volumes.

From a randomly selected subset of 15 subjects (30 orbits), seven orbital structures were manually segmented in 3D using the Amira software: (1) optic nerve, (2) globe, (3) zygomatic bone, (4) lens, (5) scleral-corneal shell, (6) rectus muscles, and (7) orbital fat (Figure 2a). The 6910 MRI slices were divided into 80% for training and validation and 20% for testing, ensuring slices from the same subject remained in the same set. Data augmentation was applied to the training data, and then a UNET model, trained with four-fold cross-validation, was used to automatically segment the entire dataset.

After segmenting the left and right eyes from each scan, the cropped-out eye orbits were reassembled to form a complete scan. The central points through the globe and lens in coronal slices were identified and fit to a central orbital axis for each eye using linear regression. This method was applicable even in myopic eyes as, to the best of our knowledge, none exhibited staphyloma. The central axial plane was then established using three points: the first two being the anterior corneal points of the left and right central orbital axes, and the third point being the midpoint between the left and right posterior poles as depicted in Figure 2b.

Axial Length. Axial length (AL) was estimated from MRI, using the distance between the cornea and posterior globe along the central orbital axis: which joined the lens and globe center^{8,9}. As such, after identifying the axial plane, AL was measured as the distance between the anterior corneal point and the posterior pole along the central orbital axis.

Globe Proptosis. Globe proptosis for each eye was calculated by measuring the distance between the anterior corneal point and the interzygomatic line. The interzygomatic line connects the most anterior points of the left and right zygomatic bone in the central axial plane.

Interzygomatic Line-to-Posterior Pole Distance. We introduced a new feature: the Interzygomatic Line-to-Posterior Pole Distance (ILPP) distance, defined as axial length minus globe proptosis. This proposed composite marker was designed to capture the interaction between globe size and proptosis. We hypothesized that ILPP distance would more closely relate to the amount of optic nerve traction experienced and provide a more nuanced understanding of orbital structure and biomechanics, and their relationship to axonal health.

Optic Nerve Tortuosity. The segmented optic nerve was skeletonized by computing the mean x and y coordinates of the optic nerve in each coronal slice to locate its center. The line was fitted to a cubic spline to reduce inter-slice noise. A 20 mm intraorbital segment was extracted beginning at the junction of the sclera and nerve, and ONT was calculated as 20 mm divided by the straight-line distance between the segment endpoints (Figure 3).

RNFL Thickness Corrected for Ocular Magnification

To correct for ocular magnification, we employed the popular Littman formula, as modified by Bennett, to adjust the RNFL thickness values. The true size of a retinal feature (t) was found by multiplying the imaging system's magnification factor (p), the ocular magnification factor (q), and the measured size (s); i.e. $t = p \times q \times s^{20-22}$. For the Topcon system, p is 3.382²². The ocular magnification factor was calculated using the formula $q = 0.01306 \times (\text{axial length} - 1.82)^{20-22}$.

Quality Control

OCT and MRI pairs with corrupted files or poor-quality scans were excluded. In the glaucoma and myopia datasets, scans hindering retinal or orbital structure visualization were manually removed following manual checks by 3D visualization. For the general population, outliers were removed using thresholding based on both Tukey's definition and biological plausibility²³. Extracted features were manually reviewed in 3D for all glaucoma and myopic subsets and selected general population subjects, with corrections applied as needed.

Statistical Analysis

Statistical analysis was conducted to evaluate the relationships between orbital features and RNFL thickness. Bivariate correlation analysis was used to assess the association between RNFL thickness and orbital features.

Generalized estimating equations (GEE) were employed to understand the combined effects of ONT and globe position and size on RNFL thickness, adjusting for age (mean of age at time of OCT and at time of MRI scan). GEE accounts for within-subject correlations in eye measurements. To minimize empirical and model-based variance estimates, an exchangeable

working correlation matrix was employed. Data was normalized before modeling. Features with a tolerance value (reciprocal of variance inflation factor) below 0.6, indicating strong multicollinearity, were excluded from the GEE. P-values below 0.05 were deemed statistically significant.

RESULTS

The UK Biobank contains 27996 pairs of OCT and MRI scans from 14617 subjects, of which 491 pairs from 250 subjects had a glaucoma diagnosis based on ICD codes. Exclusion factors were corruption of files during data extraction, poor quality data, processing errors, failure of manual checks, and thresholding. The final tally was 17970 pairs of scans with 371 pairs from glaucomatous subjects. The myopic subpopulation comprised 2481 pairs of scans. The demographic data are reported in Table 1.

The segmentation networks for both OCT and MRI achieved good performance, with Dice coefficients of 0.947 ± 0.003 and 0.954 ± 0.001 , respectively. These trained networks were then used to segment all the OCT and MRI scans before feature extraction algorithms extracted the orbital and retinal features, as shown in Table 2 and Figure 4.

General Population. In the general population, correlation analysis revealed significant positive linear relationships between ONT and corrected global RNFL thickness ($r = 0.065$, $p < 0.001$) and between ILPP distance and corrected global RNFL thickness ($r = 0.206$, $p < 0.001$) (Table 3; Figure 5). The latter was significantly stronger according to Steiger's test ($p < 0.001$)²⁴. The GEE model revealed ONT, ILPP distance, and age as significant predictors of corrected global RNFL thickness in the general population ($\beta = 0.023$, $p < 0.001$, $\beta = 0.204$, $p < 0.001$, $\beta = -0.100$, $p < 0.001$, respectively) (Table 4). These results are depicted in Figure 6.

Glaucoma Sub-population. In the glaucoma subpopulation, ONT was significantly positively correlated with corrected global RNFL thickness ($r = 0.140$, $p < 0.01$), as shown in

Table 3 and Figure 5. While this correlation was stronger than in the general population, the difference was not significant based on Fisher's Z test ($p = 0.07$). ILPP distance also showed a significant positive correlation with corrected global RNFL thickness ($r = 0.256$, $p < 0.01$). The GEE model results are depicted in Figure 6. The coefficient of ILPP distance as a predictor of corrected global RNFL thickness was statistically significant ($\beta = 0.264$, $p < 0.001$), though the coefficient of ONT was not ($\beta = 0.049$, $p = 0.31$) (Table 4),

Myopic Subpopulation. Results for the myopic subpopulation were similar to the general population with the correlation between ONT and corrected global RNFL thickness ($r = 0.071$, $p < 0.001$) being not significantly greater than the general population according to Fisher's Z test ($p = 0.4$). These findings are detailed in Tables 3 and 4 and illustrated in Figure 5.

As ILPP distance and globe proptosis exhibited multicollinearity (tolerance < 0.4), these features were not included together in any regression model (Tables 4 – 6). Models including globe proptosis can be found in Supplementary Material 1. All other pairs of independent variables had tolerance values greater than 0.6, indicating no high correlation between them. The prediction models for uncorrected global RNFL and for RNFL divided into each of the four quadrants can also be found in Supplementary Material 1.

DISCUSSION

In this study, we conducted the first population-wide investigation into orbital features and their relationship with axonal health, using corrected global RNFL thickness as a surrogate marker. Our analysis employed an AI-based medical image analysis framework with feature-based extraction to examine orbital anatomy. A novel composite metric, the ILPP distance, was introduced to account for globe proptosis and size. The results demonstrated significant positive correlations between corrected global RNFL thickness and both ONT and ILPP distance. Furthermore, these two orbital features emerged as significant predictors of corrected global RNFL thickness in GEE regression models, highlighting their potential

relevance in understanding axonal health. These findings suggest that there are critical links between the structure and possibly even biomechanics of the orbit and the retina.

Our study revealed significant correlations between less tortuous optic nerves and thinner corrected global RNFL in the general population and both disease subpopulations. This finding aligns with biomechanical principles: a straighter optic nerve has less redundancy during eye adduction, becoming taut earlier ²⁵. Once this redundancy is exhausted, the optic nerve, its sheath, and other orbital tissues likely experience greater traction forces, requiring them to stretch to accommodate eye movements ^{25,26}. These increased forces may contribute to axonal damage, which could lead to RNFL thinning, aligning with previous studies suggesting that mechanical tension and strain on the optic nerve influence axonal health and RNFL thickness ⁷⁻⁹. In eyes with glaucoma, the correlation between ONT and corrected global RNFL thickness was slightly stronger than in the general population, suggesting that straighter nerves may play a more pronounced role in exacerbating ocular neurodegeneration since these are associated with thinner RNFLs. This result aligns with Wang et al.'s report of straighter optic nerves in glaucoma patients compared to healthy controls suggesting that reduced ONT could exacerbate glaucomatous damage ⁸. Such findings highlight the role of nerve geometry in maintaining optic nerve function and its potential effect on individual susceptibility to neurodegeneration, supporting ONT as a biomarker to predict RGC axonal damage.

Moreover, we found significant positive correlations between ILPP distance and corrected global RNFL thicknesses. In the GEE models, the coefficient for ILPP distance as a predictor of corrected global RNFL thickness was also significantly positive. These findings suggest that a smaller ILPP distance, indicative of a smaller posterior segment, could induce greater traction forces on the RGC axons. We propose two potential explanations for this observation. First, a smaller ILPP distance might cause the globe-nerve junction to be more anteriorly placed. This could reduce optic nerve redundancy, impair eye movements and exacerbate RNFL thinning. This could be particularly so for glaucomatous subjects, especially during adduction, where this effect may lead to tethering as observed by Demer et al., causing globe

retraction and increasing traction forces on the optic nerve, especially at the optic nerve head¹⁰. Second, a reduced ILPP distance is correlated with increased globe proptosis, which may hinder eye movements and elevate traction forces experienced at the posterior retina. This aligns with the findings of Fisher et al., who reported increased optic nerve strain in subjects with proptosed globes⁶. It also complements the work of Wang et al., who found that both glaucoma and myopic patients exhibited more globe proptosis than healthy subjects^{8,9}. Together, these studies suggest that globe proptosis may contribute to axonal damage by increasing the mechanical strain on the optic nerve and retina.

Correction of RNFL thickness using axial length had minimal impact on the GEE model results but reversed the negative correlation between RNFL thickness and axial length in the myopic subpopulation and strengthened the weakly positive correlation between RNFL thickness and axial length in the general population and glaucoma subpopulation. This latter finding contrasts with prior studies reporting weak negative correlation pre-correction and weak positive correlation post correction^{21,22,27}. Methodological differences, participant demographics, or specific OCT devices employed may contribute to this discrepancy. Though we do note the contention that RNFL thinning by myopic axial elongation poses to this result^{27,28}, the positive correlation may reflect interactions between ILPP distance and RNFL thickness. Specifically, with the same globe proptosis, an eye with longer axial length may have a more posteriorly placed globe-nerve junction, potentially allowing more optic nerve redundancy, allowing reduced traction forces and releasing stress, thus resulting in less RNFL thinning. Further investigation is needed to better understand the complex interplay between ocular anatomy, axial length, and RNFL measurements.

In this study, several limitations warrant further discussion. First, the quality of the UK Biobank imaging data was compromised by artifacts such as shadows, blurring, and misalignment, which introduced noise. Despite excluding scans via manual checks and outlier removal, some localized errors in 3D image volumes might have gone undetected. Future studies could incorporate advanced quality control algorithms to eliminate noise, improve the overall data quality and potentially strengthen the current observed trends.

Second, the automatic segmentation algorithms were trained on a limited sample relative to the large dataset, potentially propagating errors into the feature extraction process. In particular, though 6910 image slices were used to train the MRI segmentation algorithm, these came from only 15 subjects. Additionally, multiple custom feature extraction algorithms were applied to a large volume of data. While we aimed for consistency, the sheer volume of data made it impractical to manually check the entire general population dataset for errors. Future analyses with more robust segmentation algorithms trained on larger datasets, along with advanced automated algorithms to detect segmentation errors and other data inconsistencies could strengthen the observed trends and provide even more reliable insights into the relationship between orbit features and RNFL thickness.

Third, the statistical methods used in this study, including correlation and linear GEE regression, were limited to identifying linear relationships. For instance, although axial length appeared to have the strongest linear correlation with RNFL thickness a separate test using mutual information, as detailed in Supplementary Material 1 (Note 2), suggested that ILPP distance, globe proptosis, and ONT exhibited higher dependence with RNFL thickness than axial length. This implies that the relationships exist between RNFL thickness, and these features could be non-linear in nature. While this is a limitation, our analysis effectively captured the overall trends, which are sufficient for the scope of this investigation. Future research could incorporate more advanced AI techniques to better explore these complex interactions in the orbit.

Fourth, the methods of data collection in the UK Biobank limit the generalizability of our findings. Specifically, there is a lack of information on whether glaucoma was unilateral or bilateral, and thus unilateral cases could potentially be included in the dataset. However, this limitation is mitigated by the fact that glaucoma is predominantly a bilateral disease, with studies reporting up to 90% of glaucoma patients affected bilaterally and contralateral conversion rates reaching 41.7% within two years for unilateral cases ^{29–33}.

Another limitation of the UK Biobank data collection is that many subjects had their eyes closed during MRI scanning, and not all eyes were scanned in the primary gaze position. This

could affect the measurements taken from the MRI scans, particularly ONT, adding noise to the data. However, with a large cohort, this noise could be negligible for such an exploratory study identifying preliminary trends. While the data might not be perfectly clean, it provides a strong foundation for further investigation and future algorithms to sieve out and exclude such scans could possibly strengthen the observed trends.

Finally, diagnosis information was limited to recorded ICD codes. Therefore, detailed information on disease severity and subtype was unavailable. As such, glaucoma severity, which may significantly influence RNFL thickness, was unaccounted for in our analysis. There was also significant underreporting of ICD codes for myopia in the UK Biobank, necessitating the definition based on axial length. Nonetheless, the association between thinner RNFLs and both straighter optic nerves and decreased ILPP distance in glaucoma and myopic patients remains. Normal-tension and high-tension glaucoma could also differently influence the relationship between orbital structures and retinal neurodegeneration. Future studies could be crafted to incorporate subtype-specific analysis and include disease severity which may reveal how different biomechanical forces, such as variations in ILPP distance or axial length, affect RNFL thickness in a disease-specific manner.

In conclusion, this study highlights the importance of expanding neuro-ophthalmology research to include orbital structures and biomechanics as critical factors in axonal health. Our findings suggest that ONT, globe size and proptosis play significant roles in axonal health and could provide new avenues for understanding neurodegeneration, particularly in diseases such as glaucoma and myopia. Future research examining ONT in different gaze positions and exploring the biomechanical effects on the optic nerve head could further advance our understanding of these mechanisms.

FIGURES

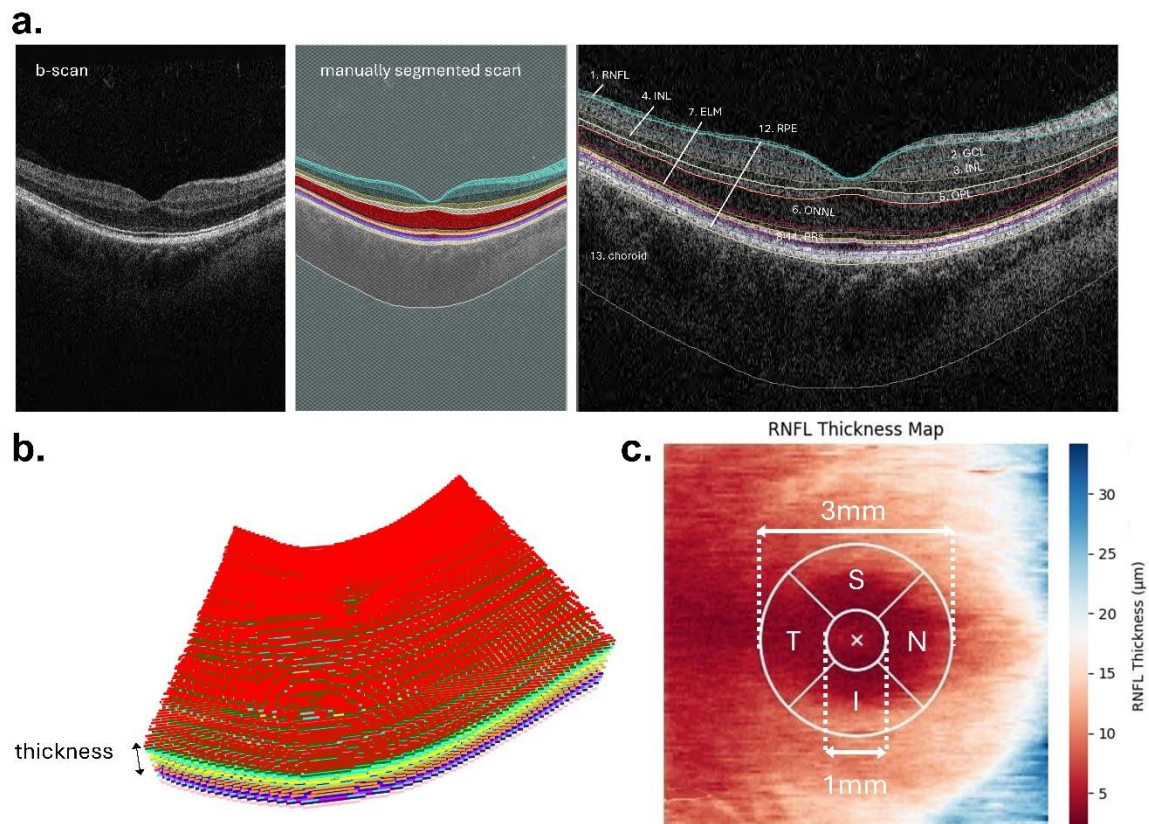


Figure 1 a. Thirteen tissue layers were manually segmented in B-scan slices from the optical coherence tomography volumes: (1) retinal nerve fiber layer (RNFL), (2) ganglion cell layer, (3) inner plexiform layer, (4) inner nuclear layer, (5) outer plexiform layer, (6) outer nuclear layer, (7) external limiting membrane, (8-11) four photoreceptor layers, (12) retinal pigment epithelium, and (13) choroid **b.** Segmented b-scans were pieced together to form the volume RNFL thickness was measured at every point of the scan area. **c.** The average thicknesses of the superior (S), nasal (N), inferior (I), and temporal (T) quadrants, and globally around the fovea were taken.

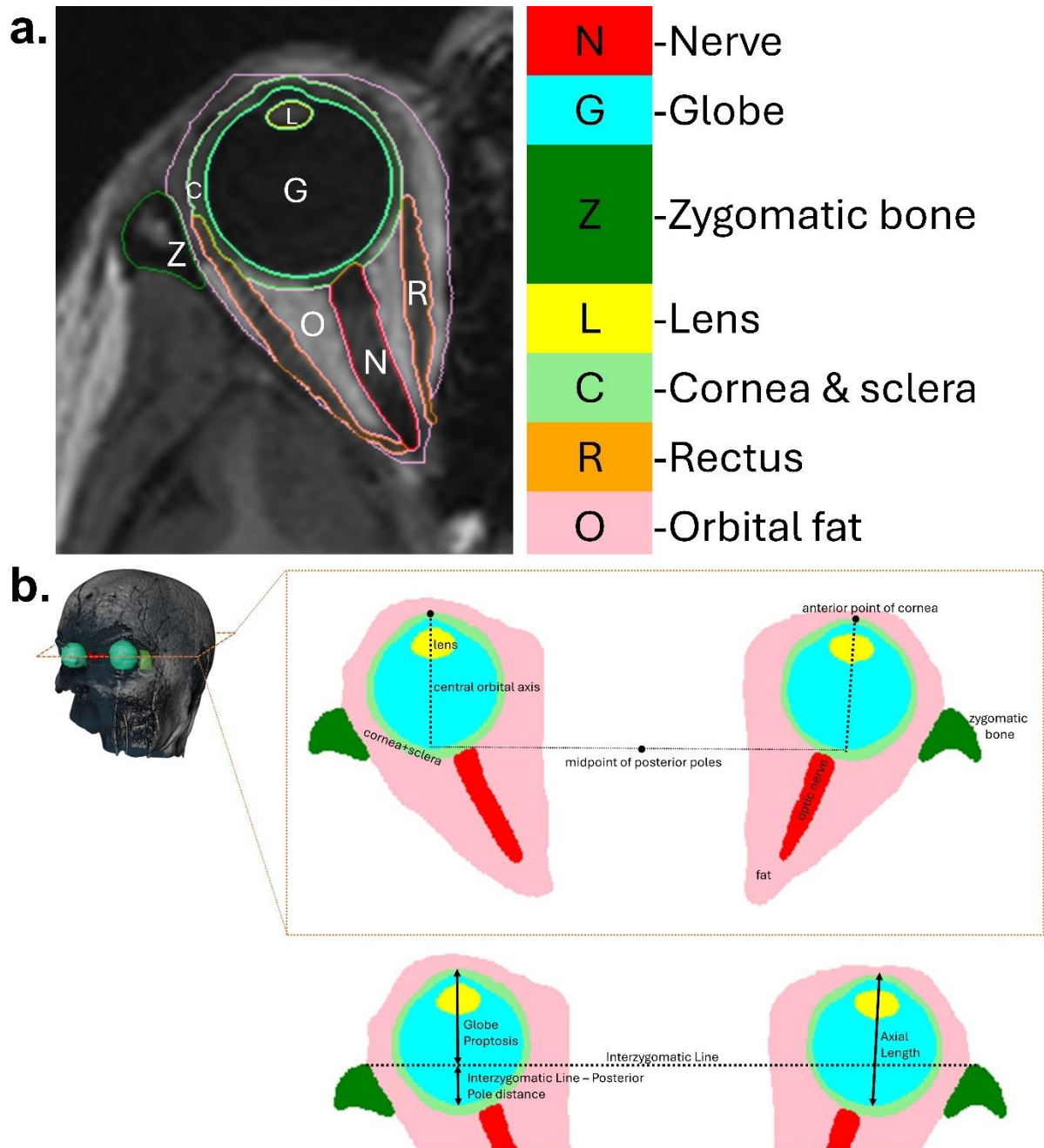


Figure 2a. Seven orbital structures were manually segmented in cropped-out orbit portions of 3D T1 brain magnetic resonance images **b.** The central axial plane was found using the anterior points of each cornea and midpoint of the posterior poles. From there, axial length was measured as the distance between the anterior cornea and posterior pole. Globe proptosis was measured from the anterior cornea to the interzygomatic line. Interzygomatic line – posterior pole distance was calculated as axial length minus globe proptosis.

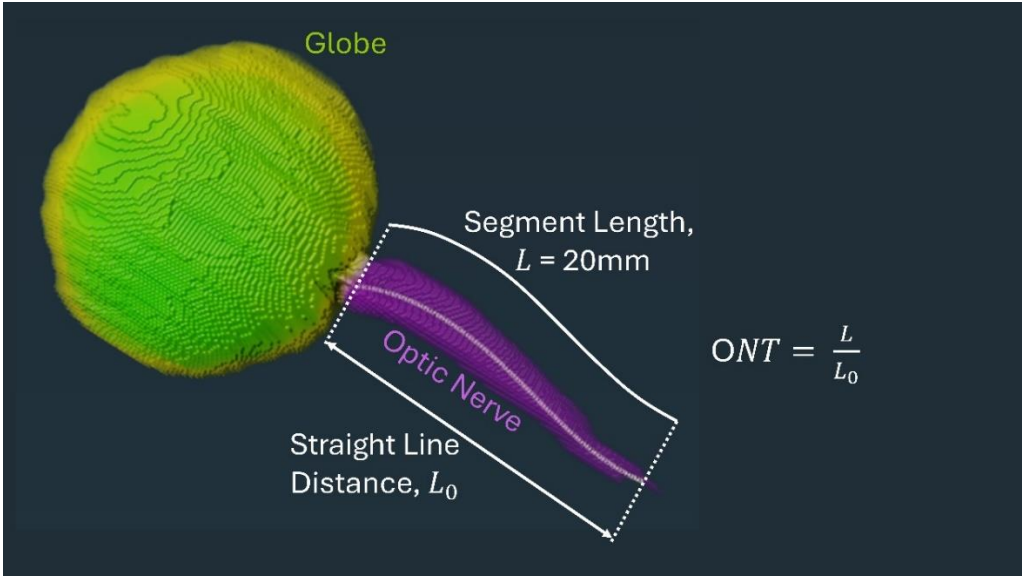


Figure 3. Optic nerve tortuosity (ONT) was taken as 20mm divided by the straight-line distance from end-to-end of a 20mm anterior segment of the skeletonized optic nerve.

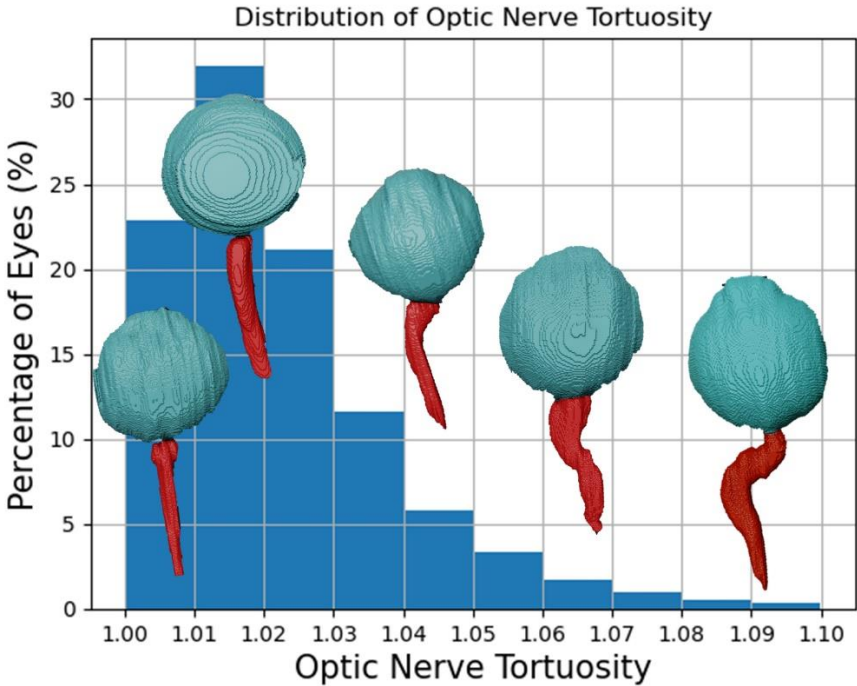
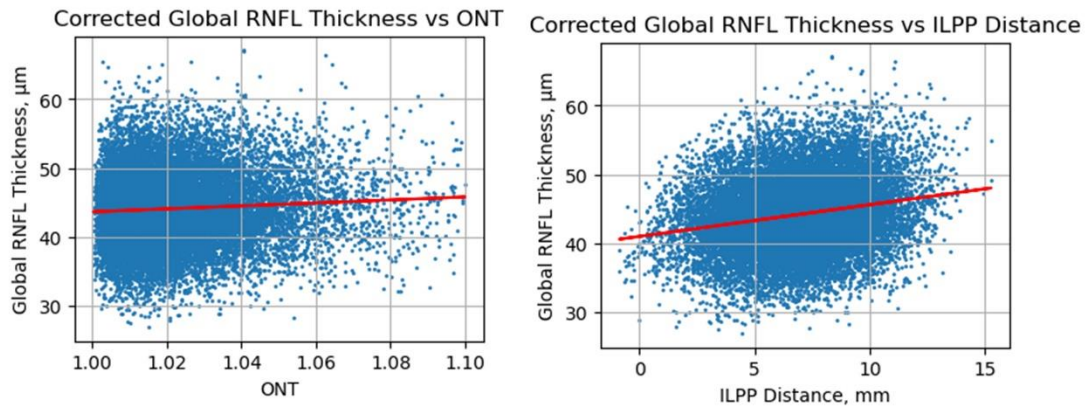
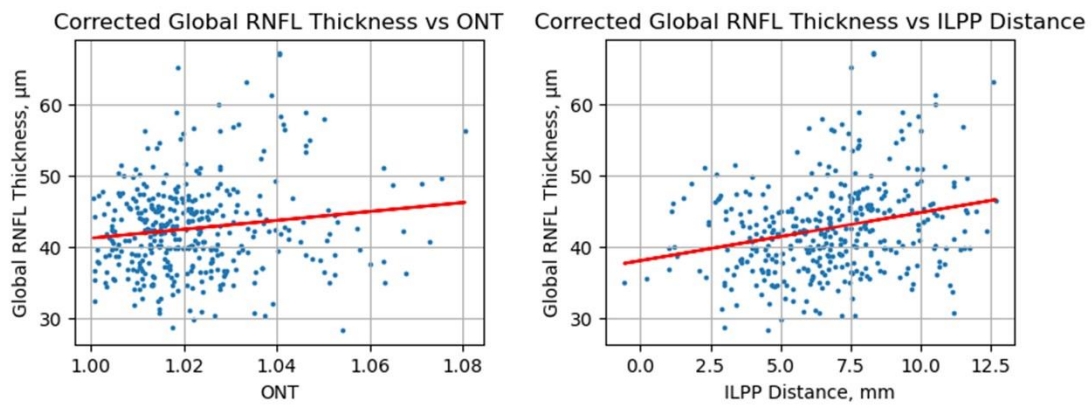


Figure 4. Distribution of optic nerve tortuosity and depiction of optic nerve geometry for different tortuosity values

General Population



Glaucoma Subpopulation



Myopic Subpopulation

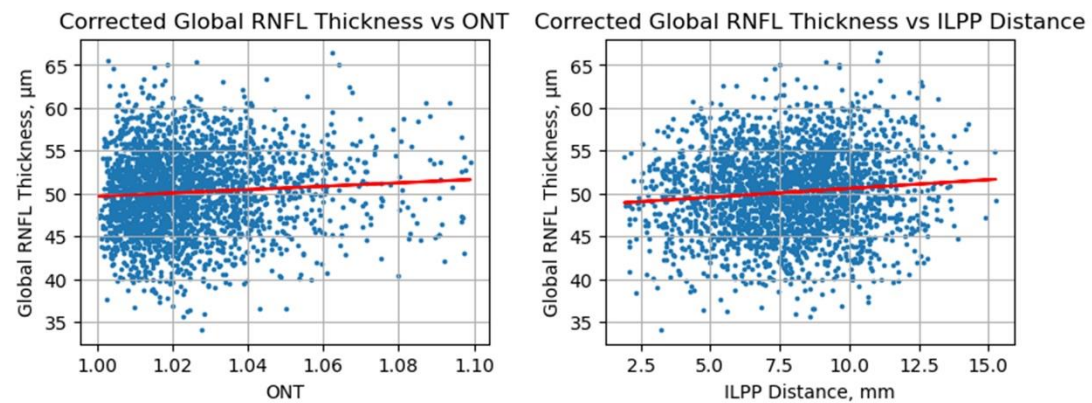


Figure 5. Corrected Global RNFL Thickness plotted against ONT and ILPP Distance in the general population and glaucoma and myopic subpopulation. RNFL, retinal nerve fiber layer; ONT, optic nerve tortuosity; ILPP, interzygomatic line-to-posterior pole.

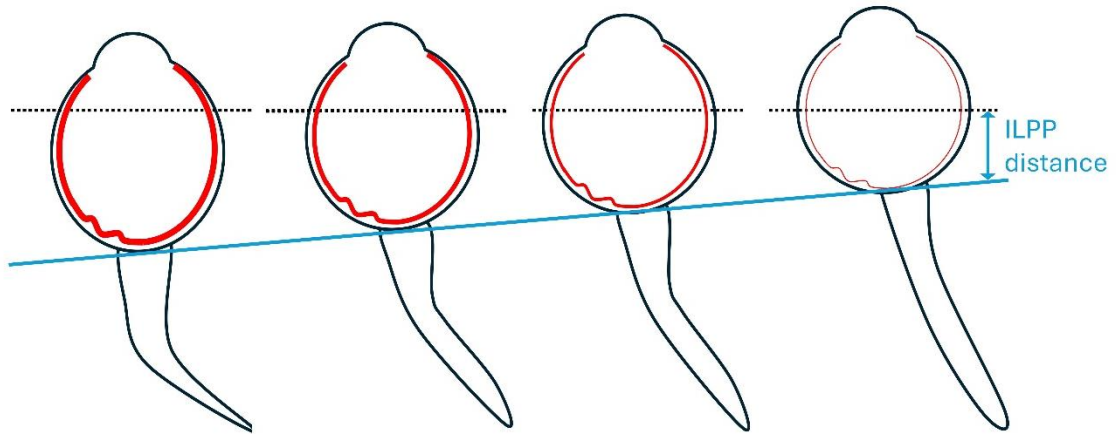


Figure 6. Retinal Nerve Fiber Layer Thinning is associated with decreased interzygomatic line-to-posterior pole (ILPP) Distance and reduced optic nerve tortuosity in the general population and both disease subpopulations.

TABLES

Table 1. Demographics of subjects from the General Population and Glaucoma Subset

	General Population	Glaucoma Subpopulation	Myopic Subpopulation
Number of participants	11531	215	1805
Gender	5758 Male, 5773 Female	129 Male, 86 Female	1172 Male, 633 Female
Number of scan pairs	17970	371	2481
Age at OCT scan, years	58.014 ± 7.833	63.270 ± 6.486	57.508 ± 7.701
Age at MRI scan, years	64.520 ± 7.756	69.218 ± 6.292	63.842 ± 7.771

Table 2. Summary of Retinal and Orbital Features

Feature	General Population	Glaucoma Subpopulation	Myopic Subpopulation
Optic Nerve Tortuosity	1.022 ± 0.016	1.022 ± 0.015	1.024 ± 0.017
ILPP Distance, mm	6.798 ± 2.353	6.730 ± 2.458	7.823 ± 2.363
Globe Proptosis, mm	16.82 ± 2.371	16.955 ± 2.343	17.883 ± 2.339
Axial Length, mm	23.619 ± 1.209	23.685 ± 1.551	25.706 ± 0.701
Age, years	61.299 ± 7.672	66.244 ± 6.245	65.549 ± 7.107
Corrected Global RNFL thickness, μ m	44.148 ± 5.263	42.566 ± 6.475	50.153 ± 4.841

Table 3. Correlation of Corrected Global RNFL Thickness with various Orbital Features

Orbital Feature	General Population		Glaucoma Subpopulation		Myopic Subpopulation	
	Pearson r	p-value	Pearson r	p-value	Pearson r	p-value
Optic Nerve Tortuosity	0.065	3×10^{-18}	0.140	0.007	0.071	4×10^{-4}
ILPP Distance	0.206	9×10^{-171}	0.256	0.007	0.100	6×10^{-7}
Globe Proptosis	0.140	1×10^{-79}	0.096	0.06	0.010	0.62
Axial Length	0.675	7×10^{-2377}	0.551	8×10^{-31}	0.370	3×10^{-81}
Age	-0.090	7×10^{-34}	-0.051	0.32	-0.068	7×10^{-4}

Table 4. Linear GEE Regression Results to Predict Corrected Global RNFL Thickness

	Coef.	Std Err	z	P> z	95% CI	
General Population						
Optic Nerve Tortuosity	0.023	0.006	3.894	1×10^{-4}	0.011	0.034
ILPP Distance	0.204	0.009	23.389	6×10^{-121}	0.187	0.221
Age	-0.100	0.010	-9.622	6×10^{-22}	-0.121	-0.08
Glaucoma Subpopulation						
Optic Nerve Tortuosity	0.049	0.048	1.023	0.31	-0.045	0.144
ILPP Distance	0.264	0.075	3.516	4×10^{-4}	0.117	0.412
Age	-0.082	0.055	-1.499	0.13	-0.189	0.025
Myopic Subpopulation						
Optic Nerve Tortuosity	0.031	0.017	1.763	0.078	-0.003	0.064
ILPP Distance	0.106	0.023	4.633	4×10^{-6}	0.061	0.151
Age	-0.063	0.025	-2.517	0.012	-0.112	-0.014

ACKNOWLEDGEMENTS

Acknowledgement is made to **(1)** This research has been conducted using data from UK Biobank, a major biomedical database; **(2)** Emory Eye Center [Start-up funds, MJAG]; **(3)** the donors of the National Glaucoma Research, a program of the BrightFocus Foundation, for support of this research (G2021010S [MJAG]); **(4)** NMRC-LCG grant 'Tackling & Reducing Glaucoma Blindness with Emerging Technologies (TARGET)', award ID: t [MJAG]; and **(5)** Support from a Challenge Grant from Research to Prevent Blindness, Inc.

REFERENCES

1. Burgoyne CF, Crawford Downs J, Bellezza AJ, Francis Suh JK, Hart RT. The optic nerve head as a biomechanical structure: a new paradigm for understanding the role of IOP-related stress and strain in the pathophysiology of glaucomatous optic nerve head damage. *Prog Retin Eye Res.* 2005;24(1):39-73. doi:10.1016/j.preteyeres.2004.06.001
2. Wang X, Fisher LK, Milea D, Jonas JB, Girard MJA. Predictions of Optic Nerve Traction Forces and Peripapillary Tissue Stresses Following Horizontal Eye Movements. *Invest Ophthalmol Vis Sci.* 2017;58(4):2044-2053. doi:10.1167/iops.16-21319
3. Shin A, Yoo L, Park J, Demer JL. Finite Element Biomechanics of Optic Nerve Sheath Traction in Adduction. *J Biomech Eng.* 2017;139(10):1010101. doi:10.1115/1.4037562
4. Wang X, Beotra MR, Tun TA, et al. In Vivo 3-Dimensional Strain Mapping Confirms Large Optic Nerve Head Deformations Following Horizontal Eye Movements. *Invest Ophthalmol Vis Sci.* 2016;57(13):5825-5833. doi:10.1167/iops.16-20560
5. Suh SY, Le A, Shin A, Park J, Demer JL. Progressive Deformation of the Optic Nerve Head and Peripapillary Structures by Graded Horizontal Duction. *Invest Ophthalmol Vis Sci.* 2017;58(12):5015. doi:10.1167/iops.17-22596
6. Fisher LK, Wang X, Tun TA, Chung HW, Milea D, Girard MJA. Gaze-evoked deformations of the optic nerve head in thyroid eye disease. *Br J Ophthalmol.* 2021;105(12):1758-1764. doi:10.1136/bjophthalmol-2020-318246
7. Demer JL, Clark RA, Suh SY, et al. Magnetic Resonance Imaging of Optic Nerve Traction During Adduction in Primary Open-Angle Glaucoma With Normal Intraocular Pressure. *Invest Ophthalmol Vis Sci.* 2017;58(10):4114-4125. doi:10.1167/iops.17-22093
8. Wang X, Rumpel H, Baskaran M, et al. Optic Nerve Tortuosity and Globe Proptosis in Normal and Glaucoma Subjects. *J Glaucoma.* 2019;28(8):691. doi:10.1097/IJG.0000000000001270

9. Wang X, Chang S, Grinband J, et al. Optic nerve tortuosity and displacements during horizontal eye movements in healthy and highly myopic subjects. *Br J Ophthalmol*. 2022;106(11):1596-1602. doi:10.1136/bjophthalmol-2021-318968
10. Demer JL, Clark RA, Suh SY, et al. Optic Nerve Traction During Adduction in Open Angle Glaucoma With Normal Versus Elevated Intraocular Pressure. *Curr Eye Res*. 2020;45(2):199-210. doi:10.1080/02713683.2019.1660371
11. Blumberg D, Skaat A, Liebmann JM. Emerging risk factors for glaucoma onset and progression. In: *Progress in Brain Research*. Vol 221. Elsevier; 2015:81-101. doi:10.1016/bs.pbr.2015.04.007
12. Kuehn M, Fingert J, Kwon Y. Retinal Ganglion Cell Death in Glaucoma: Mechanisms and Neuroprotective Strategies. *Ophthalmol Clin N Am*. 2005;18(3):383-395. doi:10.1016/j.ohc.2005.04.002
13. Betzler BK, Young SM, Sundar G. Intraocular Pressure and Glaucoma in Thyroid Eye Disease. *Ophthal Plast Reconstr Surg*. 2022;38(3):219. doi:10.1097/IOP.0000000000002049
14. Chuangsuwanich T, Tun TA, Braeu FA, et al. How Myopia and Glaucoma Influence the Biomechanical Susceptibility of the Optic Nerve Head. *Invest Ophthalmol Vis Sci*. 2023;64(11):12. doi:10.1167/iovs.64.11.12
15. McBrien NA, Jobling AI, Gentle A. Biomechanics of the Sclera in Myopia: Extracellular and Cellular Factors. *Optom Vis Sci*. 2009;86(1):E23. doi:10.1097/OPX.0b013e3181940669
16. Grytz R, Yang H, Hua Y, Samuels BC, Sigal IA. Connective Tissue Remodeling in Myopia and its Potential Role in Increasing Risk of Glaucoma. *Curr Opin Biomed Eng*. 2020;15:40-50. doi:10.1016/j.cobme.2020.01.001
17. Al-Mujaini AS, Al-Mujaini MS, Sabt BI. Retinal nerve fiber layer thickness in multiple sclerosis with and without optic neuritis: a four-year follow-up study from Oman. *BMC Ophthalmol*. 2021;21(2021):391. doi:10.1186/s12886-021-02158-0
18. Patel NB, Luo X, Wheat JL, Harwerth RS. Retinal Nerve Fiber Layer Assessment: Area versus Thickness Measurements from Elliptical Scans Centered on the Optic Nerve. *Invest Ophthalmol Vis Sci*. 2011;52(5):2477-2489. doi:10.1167/iovs.10-6105
19. Chiang CYN, Braeu FA, Chuangsuwanich T, et al. Are Macula or Optic Nerve Head Structures Better at Diagnosing Glaucoma? An Answer Using Artificial Intelligence and Wide-Field Optical Coherence Tomography. *Transl Vis Sci Technol*. 2024;13(1):5. doi:10.1167/tvst.13.1.5
20. Hirasawa K, Yamaguchi J, Nagano K, Kanno J, Kasahara M, Shoji N. Structure–Function Relationships and Glaucoma Detection with Magnification Correction of OCT Angiography. *Ophthalmol Sci*. 2022;2(2):100120. doi:10.1016/j.xops.2022.100120
21. Savini G, Barboni P, Parisi V, Carbonelli M. The influence of axial length on retinal nerve fibre layer thickness and optic-disc size measurements by spectral-domain OCT. *Br J Ophthalmol*. 2012;96(1):57-61. doi:10.1136/bjo.2010.196782

22. Kausar A, Akhtar N, Afzal F, Ali K. Effect of refractive errors/axial length on peripapillary retinal nerve fibre layer thickness (RNFL) measured by Topcon SD-OCT. *JPMA J Pak Med Assoc.* 2018;68(7):1054-1059.
23. Tukey WJ. A survey of sampling from contaminated distributions. *Contrib Probab Stat.* 1960;9(4):448-485.
24. Steiger JH. Tests for comparing elements of a correlation matrix. *Psychol Bull.* 1980;87(2):245-251. doi:10.1037/0033-2909.87.2.245
25. Clark RA, Suh SY, Caprioli J, et al. Adduction-Induced Strain on the Optic Nerve in Primary Open Angle Glaucoma at Normal Intraocular Pressure. *Curr Eye Res.* 2021;46(4):568-578. doi:10.1080/02713683.2020.1817491
26. Demer JL. Optic Nerve Sheath as a Novel Mechanical Load on the Globe in Ocular Duction. *Invest Ophthalmol Vis Sci.* 2016;57(4):1826-1838. doi:10.1167/iovs.15-18718
27. Leung CKS, Mohamed S, Leung KS, et al. Retinal Nerve Fiber Layer Measurements in Myopia: An Optical Coherence Tomography Study. *Invest Ophthalmol Vis Sci.* 2006;47(12):5171-5176. doi:10.1167/iovs.06-0545
28. Porwal S, Nithyanandam S, Joseph M, Vasnaik AK. Correlation of axial length and peripapillary retinal nerve fiber layer thickness measured by Cirrus HD optical coherence tomography in myopes. *Indian J Ophthalmol.* 2020;68(8):1584-1586. doi:10.4103/ijo.IJO_1778_19
29. Kyei S, Owusu-Afryie B, Tagoh S, Kwarteng MA, Nsiah P, Guramatunhu S. Clinical and sociodemographic characteristics of glaucoma patients at a tertiary referral facility in Zimbabwe. *Malawi Med J.* 2021;33(1):15-20. doi:10.4314/mmj.v33i1.3
30. Nam JW, Kang YS, Sung MS, Park SW. Clinical Evaluation of Unilateral Open-Angle Glaucoma: A Two-Year Follow-Up Study. *Chonnam Med J.* 2021;57(2):144-151. doi:10.4068/cmj.2021.57.2.144
31. Lee DA, Higginbotham EJ. Glaucoma and its treatment: A review. *Am J Health Syst Pharm.* 2005;62(7):691-699. doi:10.1093/ajhp/62.7.691
32. Kim C, Kim TW. Comparison of Risk Factors for Bilateral and Unilateral Eye Involvement in Normal-Tension Glaucoma. *Invest Ophthalmol Vis Sci.* 2009;50(3):1215-1220. doi:10.1167/iovs.08-1886
33. Popović V. The Glaucoma Population in Gothenburg. *Acta Ophthalmol (Copenh).* 1982;60(5):745-758. doi:10.1111/j.1755-3768.1982.tb06735.x

SUPPLEMENTARY MATERIAL 1

Supplementary Table 1. Correlation of Global Retinal Nerve Fiber Layer (RNFL) Thickness with various Orbital Features

Orbital Feature	General Population		Glaucoma Subpopulation		Myopic Subpopulation	
	Pearson r	p-value	Pearson r	p-value	Pearson r	p-value
Optic Nerve Tortuosity	0.049	4×10^{-11}	0.105	0.04	0.055	0.006
ILPP Distance	0.121	6×10^{-60}	0.091	0.08	0.049	0.02
Globe Proptosis	0.020	0.008	-0.027	0.61	-0.028	0.16
Axial Length	0.275	2×10^{-309}	0.103	0.05	0.073	4×10^{-4}
Age	-0.102	1×10^{-42}	-0.050	0.34	-0.073	2×10^{-4}

Supplementary Table 2. Correlation of Retinal Nerve Fiber Layer (RNFL) Thicknesses in 4 Quadrants with Orbit Features in the General Population

Retinal Feature	Orbital Feature	Pearson r	p-value
Superior RNFL Thickness	Optic Nerve Tortuosity	0.047	2×10^{-10}
	ILPP Distance	0.100	4×10^{-41}
	Globe Proptosis	0.006	0.43
	Axial Length	0.206	1×10^{-171}
	Age	-0.079	3×10^{-26}
Corrected Superior RNFL Thickness	Optic Nerve Tortuosity	0.063	3×10^{-17}
	ILPP Distance	0.180	1×10^{-130}
	Globe Proptosis	0.111	1×10^{-50}
	Axial Length	0.569	2×10^{-1530}
	Age	-0.076	2×10^{-24}
Inferior RNFL Thickness	Optic Nerve Tortuosity	0.038	4×10^{-7}
	ILPP Distance	0.088	3×10^{-32}
	Globe Proptosis	0.015	0.04
	Axial Length	0.201	8×10^{-163}
	Age	-0.109	2×10^{-48}
Corrected Inferior RNFL Thickness	Optic Nerve Tortuosity	0.054	3.38E-13
	ILPP Distance	0.165	4×10^{-110}
	Globe Proptosis	0.114	1×10^{-52}
	Axial Length	0.545	3×10^{-1379}
	Age	-0.103	2×10^{-43}
Temporal RNFL Thickness	Optic Nerve Tortuosity	0.036	2×10^{-6}
	ILPP Distance	0.050	1×10^{-11}
	Globe Proptosis	0.031	4×10^{-5}
	Axial Length	0.158	6×10^{-101}
	Age	-0.043	1×10^{-8}
Corrected Temporal RNFL Thickness	Optic Nerve Tortuosity	0.065	3×10^{-18}
	ILPP Distance	0.206	9×10^{-171}
	Globe Proptosis	0.140	1×10^{-79}
	Axial Length	0.675	7×10^{-2377}
	Age	-0.090	7×10^{-34}
Nasal RNFL Thickness	Optic Nerve Tortuosity	0.040	6×10^{-8}
	ILPP Distance	0.144	3×10^{-84}
	Globe Proptosis	0.024	0.001
	Axial Length	0.328	5×10^{-448}
	Age	-0.082	5×10^{-28}

Corrected Nasal RNFL Thickness	Optic Nerve Tortuosity	0.056	8×10^{-14}
	ILPP Distance	0.212	1×10^{-181}
	Globe Proptosis	0.126	8×10^{-65}
	Axial Length	0.660	6×10^{-2236}
	Age	-0.075	4×10^{-24}

Supplementary Table 3. Linear Generalized Estimating Equation Regression Models to Predict Global Retinal Nerve Fiber Layer (RNFL) Thickness

	Coef.	Std Err	z	P> z	95% CI	
General Population						
Optic Nerve Tortuosity	0.024	0.006	3.913	9×10^{-5}	0.012	0.036
ILPP Distance	0.108	0.009	12.436	2×10^{-35}	0.091	0.125
Age	-0.111	0.010	-10.875	2×10^{-27}	-0.131	-0.091
Glaucoma Subpopulation						
Optic Nerve Tortuosity	0.064	0.054	1.185	0.24	-0.042	0.171
ILPP Distance	0.082	0.081	1.013	0.31	-0.077	0.241
Age	-0.074	0.054	-1.377	0.17	-0.179	0.031
Myopic Subpopulation						
Optic Nerve Tortuosity	0.027	0.018	1.546	0.122	-0.007	0.062
ILPP Distance	0.050	0.023	2.166	0.03	0.005	0.095
Age	-0.067	0.025	-2.661	0.008	-0.116	-0.018

Supplementary Table 4. Linear Generalized Estimating Equation Regression Models to Predict Global Retinal Nerve Fiber Layer (RNFL) Thickness using Globe Proptosis and Axial Length in the General Population

	Coef.	Std Err	z	P> z	95% CI	
Prediction of Global RNFL Thickness						
Optic Nerve Tortuosity	0.0239	0.006	3.93	9×10^{-5}	0.012	0.036
Globe Proptosis	-0.0455	0.009	-5.219	2×10^{-7}	-0.063	-0.028
Axial Length	0.2679	0.009	30.728	2×10^{-207}	0.251	0.285
Age	-0.1057	0.01	-10.717	8×10^{-27}	-0.125	-0.086
Prediction of Corrected Global RNFL Thickness						

Optic Nerve Tortuosity	0.023	0.005	4.849	1×10^{-6}	0.014	0.033
Globe Proptosis	-0.034	0.007	-4.987	6×10^{-7}	-0.048	-0.021
Axial Length	0.672	0.007	95.411	0	0.658	0.686
Age	-0.086	0.008	-11.096	1×10^{-28}	-0.101	-0.071

Supplementary Table 5 Linear Generalized Estimating Equation Regression Models to Predict Global Retinal Nerve Fiber Layer (RNFL) Thickness using Globe Proptosis and Axial Length in the Glaucoma Sub-population

	Coef.	Std Err	z	P> z	95% CI	
Prediction of Global RNFL Thickness						
Optic Nerve Tortuosity	0.064	0.055	1.178	0.24	-0.043	0.171
Globe Proptosis	-0.036	0.078	-0.463	0.64	-0.188	0.116
Axial Length	0.124	0.072	1.726	0.08	-0.017	0.266
Age	-0.066	0.054	-1.232	0.22	-0.172	0.039
Prediction of Corrected Global RNFL Thickness						
Optic Nerve Tortuosity	0.050	0.045	1.102	0.27	-0.039	0.138
Globe Proptosis	-0.034	0.064	-0.535	0.59	-0.159	0.091
Axial Length	0.563	0.062	9.044	2×10^{-19}	0.441	0.685
Age	-0.046	0.045	-1.011	0.31	-0.135	0.043

Supplementary Table 6. Linear Generalized Estimating Equation Regression Models to Predict Global Retinal Nerve Fiber Layer (RNFL) Thickness using Globe Proptosis and Axial Length in the Myopic Sub-population

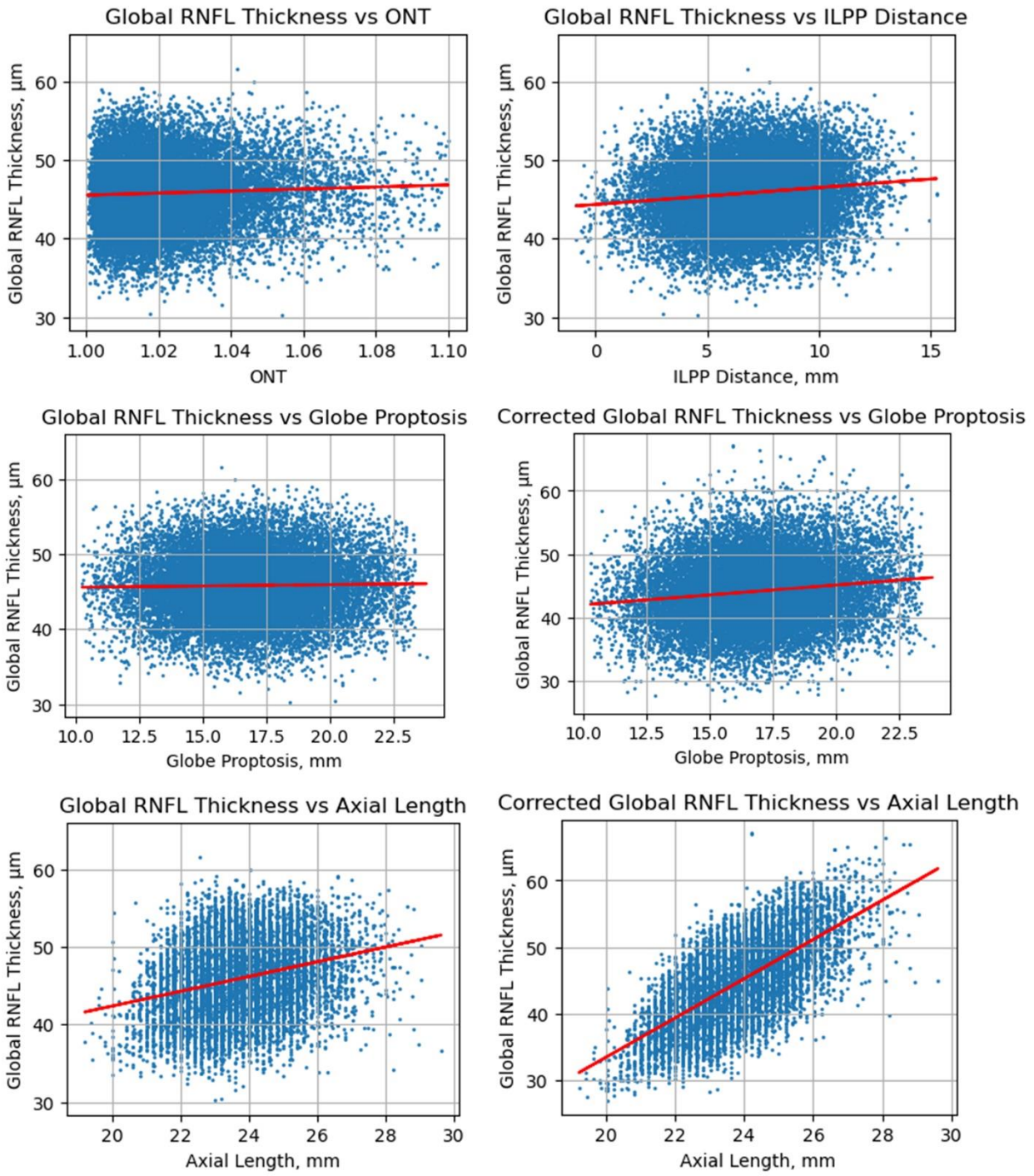
	Coef.	Std Err	z	P> z	95% CI	
Prediction of Global RNFL Thickness						
Optic Nerve Tortuosity	0.025	0.018	1.378	0.17	-0.01	0.059
Globe Proptosis	-0.034	0.023	-1.45	0.15	-0.079	0.012
Axial Length	0.055	0.02	2.715	0.01	0.015	0.094
Age	-0.065	0.025	-2.61	0.01	-0.114	-0.016
Prediction of Corrected Global RNFL Thickness						
Optic Nerve Tortuosity	0.011	0.017	0.67	0.50	-0.022	0.044

Globe Proptosis	-0.035	0.022	-1.581	0.11	-0.077	0.008
Axial Length	0.294	0.02	14.75	3×10^{-49}	0.255	0.333
Age	-0.055	0.024	-2.338	0.02	-0.101	-0.009

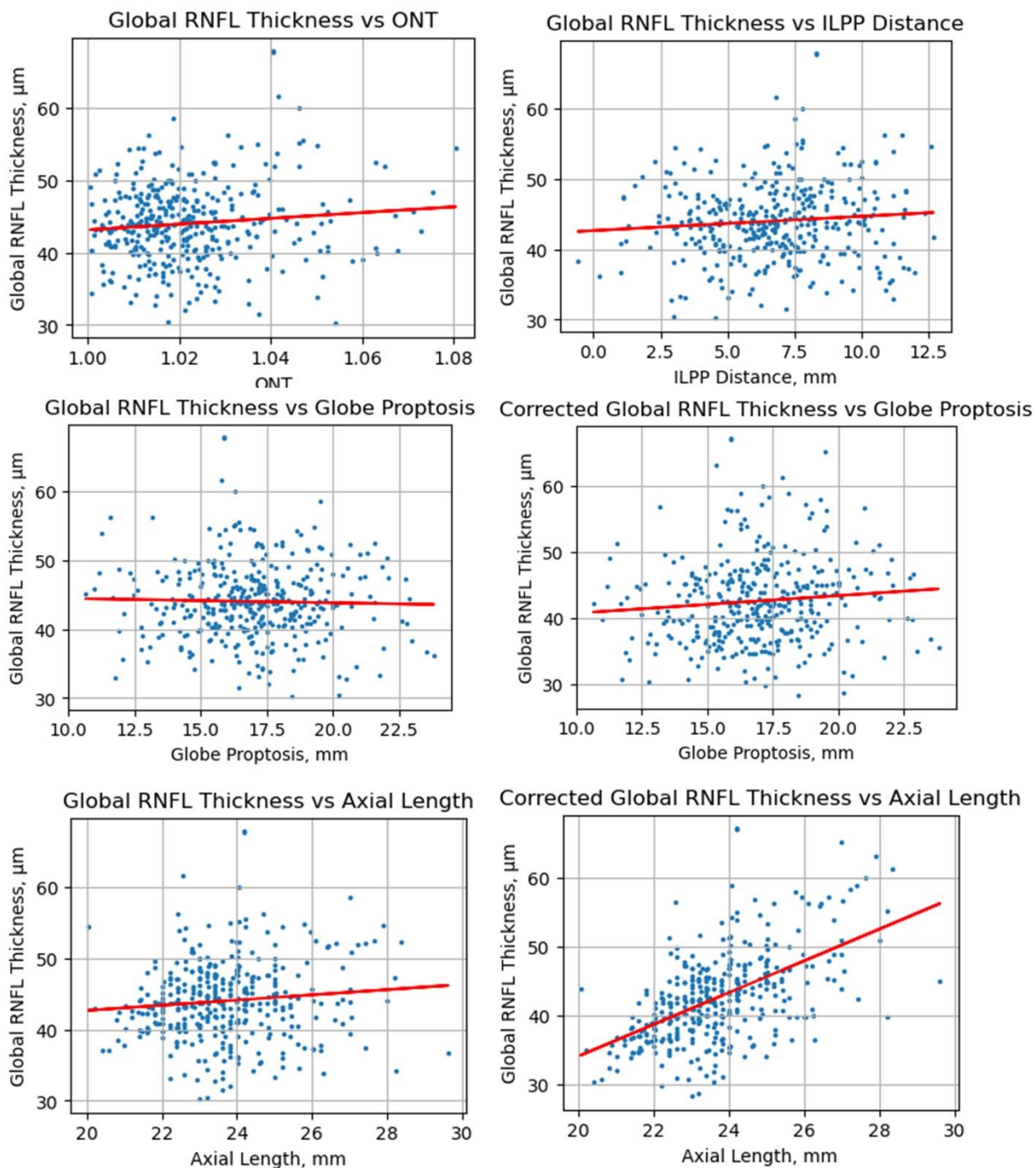
Supplementary Table 7. Linear Generalized Estimating Equation Regression Models to Predict Retinal Nerve Fiber Layer (RNFL) Thickness in 4 Quadrants in the General Population

	Coef.	Std Err	z	P> z 	95% CI	
Prediction of Superior RNFL Thickness						
Optic Nerve Tortuosity	0.025	0.007	3.639	2×10^{-4}	0.011	0.038
ILPP Distance	0.090	0.009	10.183	2×10^{-24}	0.072	0.107
Age	-0.088	0.01	-8.731	3×10^{-18}	-0.108	-0.069
Prediction of Corrected Superior RNFL Thickness						
Optic Nerve Tortuosity	0.023	0.007	3.476	0.001	0.01	0.036
ILPP Distance	0.178	0.009	19.853	1×10^{-87}	0.16	0.195
Age	-0.086	0.01	-8.243	2×10^{-16}	-0.106	-0.065
Prediction of Inferior RNFL Thickness						
Optic Nerve Tortuosity	0.021	0.021	0.021	0.021	0.021	0.021
ILPP Distance	0.078	0.078	0.078	0.078	0.078	0.078
Age	-0.124	-0.124	-0.124	-0.124	-0.124	-0.124
Prediction of Corrected Inferior RNFL Thickness						
Optic Nerve Tortuosity	0.024	0.007	3.614	3×10^{-4}	0.011	0.037
ILPP Distance	0.160	0.009	18.06	7×10^{-73}	0.143	0.177
Age	-0.117	0.01	-11.299	1×10^{-29}	-0.137	-0.096
Prediction of Temporal RNFL Thickness						
Optic Nerve Tortuosity	0.028	0.028	0.028	0.028	0.028	0.028
ILPP Distance	0.042	0.042	0.042	0.042	0.042	0.042
Age	-0.051	-0.051	-0.051	-0.051	-0.051	-0.051
Prediction of Corrected Temporal RNFL Thickness						
Optic Nerve Tortuosity	0.021	0.006	3.286	0.001	0.008	0.033
ILPP Distance	0.175	0.009	19.563	3×10^{-85}	0.157	0.192
Age	-0.051	0.01	-4.903	9×10^{-7}	-0.071	-0.031
Prediction of Nasal RNFL Thickness						
Optic Nerve Tortuosity	0.019	0.007	2.788	0.005	0.006	0.032
ILPP Distance	0.135	0.009	15.398	2×10^{-53}	0.118	0.152
Age	-0.092	0.01	-9.126	7×10^{-20}	-0.112	-0.072
Prediction of Corrected Nasal RNFL Thickness						

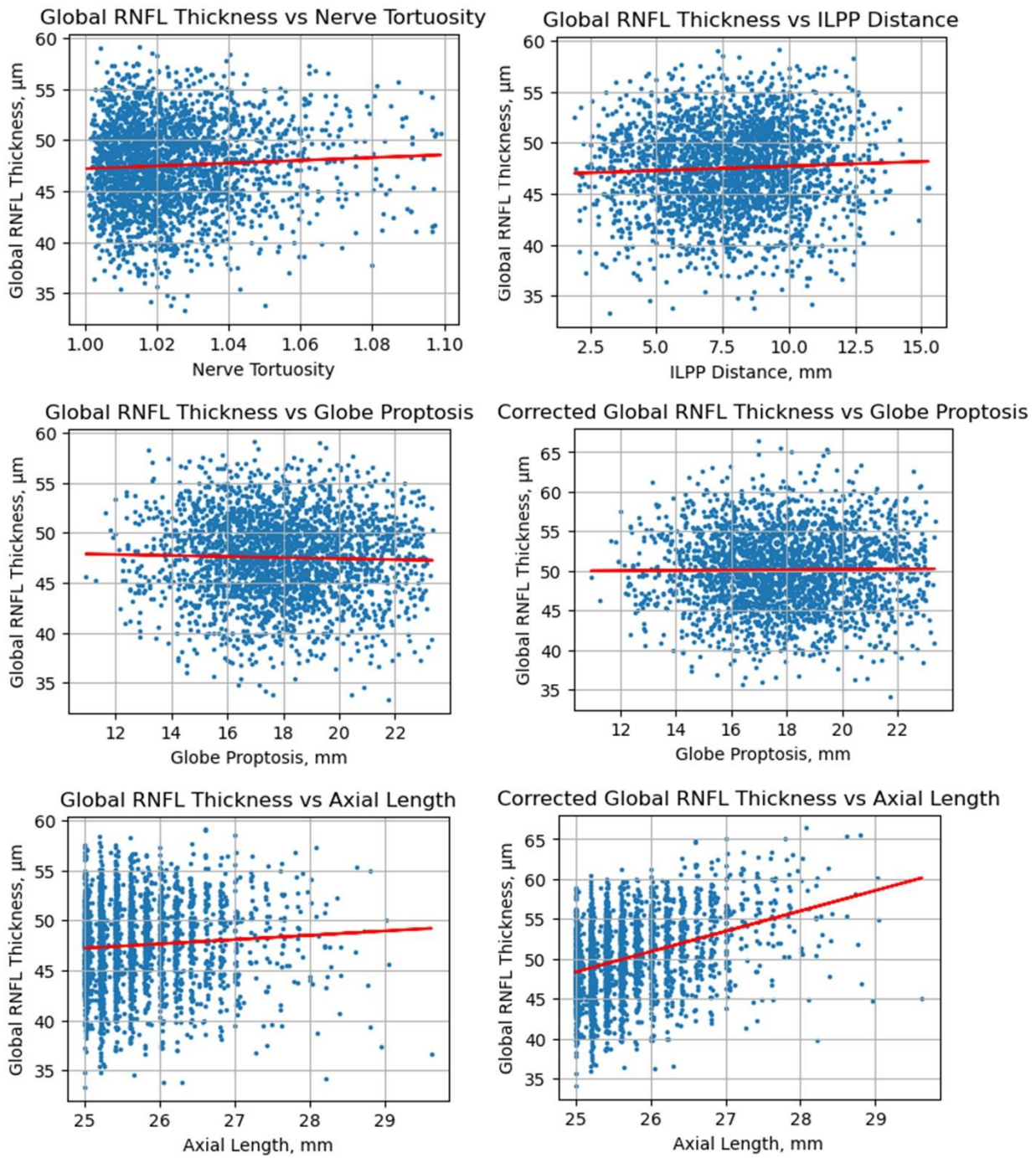
Optic Nerve Tortuosity	0.021	0.006	3.195	0.001	0.008	0.033
ILPP Distance	0.210	0.009	23.512	3×10^{-122}	0.192	0.227
Age	-0.086	0.01	-8.316	9×10^{-17}	-0.106	-0.066



Supplementary Figure 1. Scatter plots of Retinal Nerve Fiber Layer (RNFL) thickness, with and without correction for ocular magnification, against features of the orbit in the general population



Supplementary Figure 2. Scatter plots of Retinal Nerve Fiber Layer (RNFL) thickness, with and without correction for ocular magnification, against features of the orbit in the glaucoma subpopulation



Supplementary Figure 3. Scatter plots of Retinal Nerve Fiber Layer (RNFL) thickness, with and without correction for ocular magnification, against features of the orbit in the myopic subpopulation

Supplementary Note 1.

In the UKBiobank, subjects identified as having glaucoma were subjects tagged with one or more of the following International Classification of Disease (ICD) codes as detailed in Supplementary Table 8.

Supplementary Table 8. ICD Codes for Glaucoma

ICD Code	ICD Code Description
ICD-9 Codes	
3651	Open-angle glaucoma
3652	Primary angle-closure glaucoma
3659	Glaucoma NOS: Unspecified glaucoma
ICD-10 Codes	
H400	Glaucoma suspect
H401	Primary open-angle glaucoma
H402	Primary angle-closure glaucoma
H408	Other glaucoma
H409	Glaucoma, unspecified

Supplementary Note 2.

Mutual information scores were used to evaluate the dependence between variables. Mutual information captures non-linear relationships and is thus, useful for detecting non-linear dependencies that might be missed by correlation-based methods. While the absolute values of mutual information scores are arbitrary, they can be used to compare the relative importance of features within a specific dataset by calculating mutual information between a target variable and each feature. A score of 0 indicates independence, while higher scores indicate stronger dependence.

The mutual information scores, as shown in Supplementary Table 8, indicated that Globe Proptosis and interzygomatic line-to-posterior pole (ILPP) Distance had similar amounts of mutual information with RNFL thickness, as well as having the most mutual information with RNFL thickness compared to other orbit features (Supplementary Table 9). Nerve tortuosity followed closely in the ranking of features sharing most mutual information with RNFL thicknesses. These results were true for both the general population and glaucoma subpopulation.

Supplementary Table 9. Mutual Information Scores of Orbit Features with Global RNFL Thickness

Rank	Orbital Feature	General Population	Glaucoma Sub-population	Myopic Sub-population
1	Globe Proptosis	2.91	5.09	4.36
2	ILPP Distance	2.74	5.07	4.32
3	Nerve Tortuosity	2.63	5.00	4.18
4	Axial Length	1.50	4.27	4.05
5	Age	0.86	3.23	3.54

As Globe Proptosis and ILPP Distance were highly collinear, only one could be included as a predictor in the GEE model. Given that Globe Proptosis and ILPP Distance both had similar amounts of mutual information with RNFL thickness, but ILPP Distance was significantly more strongly correlated with RNFL thickness than Globe Proptosis (Tables 3 and

4), i.e. stronger linear relationship, thus, ILPP distance was included as a predictor in the linear GEE model rather than Globe Proptosis.